Microfabricated porous SU-8 membranes as innervation interfaces for hiPSC-neurons in microfluidic devices

Journal of Physics Communications

OPEN ACCESS

RECEIVED
13 September 2021

REVISED
10 October 2021

ACCEPTED FOR PUBLICATION
20 October 2021

PUBLISHED
1 November 2021

PAPER

Microfabricated porous SU-8 membranes as innervation interfaces for hiPSC-neurons in microfluidic devices

T Salpavaara[1], **T Joki**[1], **A Skogberg, M T Calejo, J Lekkala, S Narkilahti and P Kallio**

Faculty of Medicine and Health Technology, Tampere University, Tampere, Finland
[1] Equal contribution.

E-mail: timo.salpavaara@tuni.fi

Keywords: microfabrication, porous membrane, cell culture model, neuron

Supplementary material for this article is available online

Abstract

In this study, we developed microfabricated porous membranes aimed at facilitating innervation in 3D cell culture models. The aim of the paper is to introduce a fabrication method for porous membranes with adjustable size, shape and location of the pores without obstructing imaging or the connectivity of the cells. The method is based on making a patterned SU-8 layer on a sacrificial aluminium layer by UV lithography and releasing it with etching. With the proposed method, we were able to produce single-layer self-supporting membranes that were used as interfaces in compartmentalized microfluidic devices. The functionality of the membranes and their cytocompatibility were tested by culturing human pluripotent stem cell (hPSC)-derived neurons on their surfaces. *In vitro* experiments demonstrated that a dense neural network develops on top of the proposed membranes within a week. Neurites were able to migrate through the pores to the bottom side of the membranes. We achieved partial, but still significant, axonal isolation. The results of this study will pave the way for the development of optimized innervated tissue models by using the combination of porous SU-8 membrane substrates, microelectrode arrays and hPSC-derived neurons in compartmentalized cell cultivation devices.

1. Introduction

Different types of engineered cell culture devices and chips are currently utilized as tools for building next-generation cell and tissue models *in vitro*. The cultures of multiple cell types are often separated by interfaces or barriers to achieve better control over the environment in each compartment. Compartmentalization has been achieved with microtunnels in horizontal 2D models [1, 2] or by using microporous membranes in three-dimensional (3D) vertical models [3]. One of the main benefits of compartmentalization is flow isolation, which allows the use of different cell media and targeted drug delivery in separate compartments [4].

Microporous membranes can be utilized as barriers in 3D cell and tissue models, including organ- and body-on-chip models, and are a very appealing research area for multiple applications [5, 6]. The membranes have been used for studying cell migration [7], humoral effects [8] and filtration between compartments [3]. Membranes have been used for modelling interfaces in the body, such as the surface of the lungs [9], blood-brain barrier [10] and gut [11]. The suitability of a certain membrane for the indented application depends on its characteristics such as pore size, pore density, material and membrane thickness.

In neuronal *in vitro* applications, compartmentalization is utilized to establish guided axonal growth from a neuronal soma compartment to an adjacent compartment to create either a neuronal network for connectivity models [12, 13] or models for target tissue innervation [14, 15]. 2D microtunnels have been increasingly utilized in axonal isolation studies [16]. Fewer studies have been reported on innervation by using membranes [5].

Membranes separating compartments are also practical substrates for placing sensors, for example, for monitoring the incubation conditions, tissue-specific functionality or the interaction of cells between the

compartments. For example, electrical interactions can be measured with perforated microelectrode arrays (MEAs). The perforated MEAs are membrane structures incorporating electrodes and openings [17]. Similar structures can be stacked into 3D micro-electrode arrays [18]. The electrodes can be also located inside the tissue blocks by using flexible 2D mesh, for example [19, 20]. The true electrical 3D measurements inside tissue blocks are possible with dense nanofabricated neural probes [21]. There is a trend to incorporating electrical measurements in 3D cell culture experiments [22]. Another important aspect in the implementation of feasible interface structures in cell applications is their effect on microscopy and other optical sensors. Thus, the membranes should be transparent; the used material should not have significant autofluorescence, and an excessive relief on the surface should be avoided.

The microporous membranes have been fabricated by track-etching ready-made polyethylene (PET) or polycarbonate (PC) films [23] or by patterning films on sacrificial layers using photolithography and releasing them by etching the layers. An alternative option is to use electrospun materials [24]. The microporous membranes in commercial cell culture inserts or transwell migration assays are often fabricated by a track-etching method. The challenge of this method is that the pore distribution is irregular and that there is no easy way to adjust the location, shape, or exact orientation of the pores. In addition, the thickness of these membranes is typically much larger than the pore diameter. Thus, the etched tracks form long narrow tunnels in the membrane [5]. These membranes with irregular pore distribution are not feasible substrates for building small sensors, such as MEAs, on their surfaces to monitor cellular interactions through the membrane.

In contrast, photolithography-based methods allow direct patterning of the pores in the membranes made of photosensitive materials such as SU-8 and 1002F photoresists [25, 26]. Alternatively, photolithography can be used to pattern a mask layer over common membrane materials such as parylene [26, 27] or polydimethylsiloxane (PDMS) [7] to dry-etch the pores. Ultraviolet (UV) lithography enables direct positioning of the pores, multiple stacked layers of photoresist in the same membrane and implementing MEAs between the layers [19, 20]. The limitation of this method in comparison with track-etching is the fabrication of sufficiently small pores due to the material constrains and accuracy of the masking techniques. However, Kim *et al* tested a method for fabricating 0.8 μm to 4 μm pores in 1 μm thick 1002 F photoresist membranes with UV lithography [26]. Warkiani *et al* were able to fabricate pores with a mean size of 1.5 μm in a 4 μm thick SU-8 membrane [28]. The very thin membranes are hard to manipulate and may not be fully self-supporting, as demonstrated in the publication of Esch *et al* [25]. Thus, both of the aforementioned groups used additional reinforcements to support their membranes. However, Quirós-Solano *et al* were able to fabricate 2 μm pores to PDMS membranes by using a dry-etching method without supporting layers [7].

The dispersion of UV light limits the resolution of standard UV lithography to dimensions of approximately 1 μm. There are some tested methods for improving the resolution of the features in the membranes. Kuiper *et al* tested the use of interference lithography for the fabrication of 0.1 μm diameter pores in silicon nitride [29]. Another possibility for fabricating precise pores in the membranes is to use e-beam lithography [30]. The interference lithography requires much complicated mask arrangement, and the e-beam lithography is a relatively time-consuming process and requires special equipment. Submicron features such as holes can also be fabricated on SU-8 surfaces using nanoimprint methods and deep reactive ion etching technologies [31]. The hindrance of this method is the fabrication of the needed high-detail imprint mould.

A sacrificial layer is needed to release the patterned membrane. The material of this layer determines the viable etchant/solvent and the possible residues, which may cause problems [7]. The membranes build on soap-based layers can be released in water [26]. Warkiani *et al* tested various polymer release layers, such as AZ 9260 photoresist and polystyrene and the corresponding solvents including acetone and toluene. In addition, the compatibility of the membrane fabrication process with the other possible processes such as sensor/wiring fabrication has to be taken account. Some release chemicals can swell the membrane substrate material, or the patterning process of the wiring may compromise the release layer. Metallic release layers such as nickel [19, 20] are common in the fabrication processes where the electrical wirings are fabricated on top of the released structure.

We studied porous SU-8 membranes as interface layers for human induced pluripotent stem cells (hiPSCs) derived neuronal cells. The purpose of the layer is to support the cells which will innervate the tissue under the membrane in 3D microfluidic cell cultures. The hiPSCs-derived neurons are presently considered a highly relevant cells for organ- and body-on-chip applications since they can be generated in a high numbers and they resable the human brain neurons better than rodent- or tumour-derived neurons. In the current literature, the most axonal isolation studies have been conducted with rodent cells [16]. To our knowledge, the behaviour of neurites of hiPSC-derived neurons has not been adequately studied on porous SU-8 membranes. These cells and their processes are sensitive to the environment and substrate materials, and thus, cytocompatibility has to be proven for each case. The use of valid cell types possessing cell type-specific behaviour is absolutely crucial when building relevant *in vitro* models both for organ-on-chip applications and for more complex body-on-chip approaches, including innervation. The differences in behaviour are, in addition to *in vivo*, also detectable

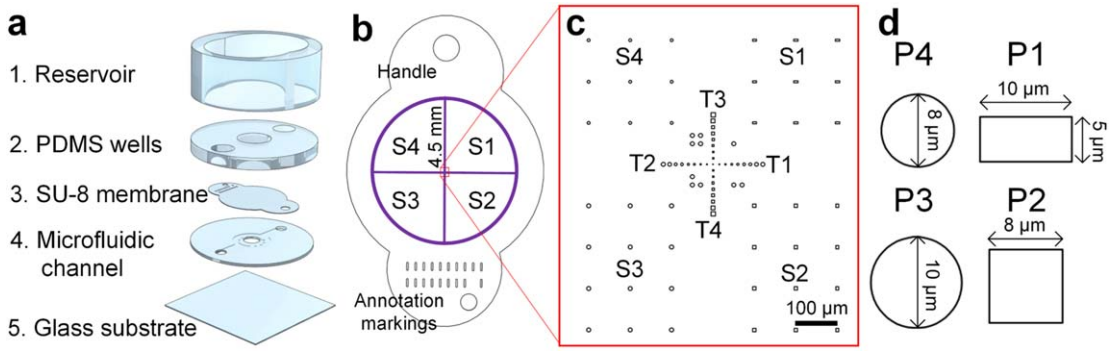

Figure 1. (a) Exploded view of the microfluidic cell culture device with description of each part. (b) The SU-8 membrane was divided into four test sectors each containing one pore type. (c) The pores were placed in the sectors in grid formations with 100 μm separation. In addition, there was a quality control test pattern in the middle of the membrane. (d) The dimensions of the designed pores.

in vitro as previously shown [32, 33]. In the case of neurons, demonstrating cell type-specific behaviour necessitates the measurement of the electrical activity in single cells and the neuronal network activity [34–36].

In this paper, we developed a microfabrication method for making porous self-supporting single-layer SU-8 membranes with regular and controlled pore size, shape, and distribution. The sacrificial layer in our fabrication process was selected in such a way that it will facilitate the fabrication of a sensor layer on top of the membrane to measure electrical functionality of the neuronal cells in the future and is still feasible to remove. In addition to the membrane fabrication process, we developed a method for assembling these membranes into stacked microfluidic cell culture devices. Instead of building thick rigid supporting layers on the membranes, we tested a method where the released thin SU-8 structures were straightened out using the surface tension of water and handled by utilizing their adhesion to pervious strips. The basic functionality of the membranes was verified in this paper by culturing hiPSC-derived neurons on them. The goal was to create a membrane that can be used as a multifunctional and controllable interface structure that meets different claims of multicell cultivation.

2. Methods

2.1. Microfluidic device

In this study, we tested porous SU-8 membranes in a compartmentalized cell culture device. Neurons were plated in a PDMS well on top of the membrane, and their neurites were able to migrate through the pores into a microfluidic channel underneath the well. The device consisted of five stacked parts (figure 1(a)): a medium reservoir (Part 1), PDMS wells (Part 2), porous SU-8 membrane (Part 3), microfluidic channel (Part 4) and glass substrate (Part 5). Parts 1, 2 and 4 were made of polydimethylsiloxane (PDMS) (Sylgard 184, Dow Corning), and the dimensions of these parts are given in the supplementary figure 1 (available online at stacks.iop.org/JPCO/5/115003/mmedia). The medium reservoir ensured proper nutrient flow to the cells without active perfusion. The PDMS wells (Part 2) had three punctured holes. Cells were injected in the middle hole on top of the membrane, and the side holes were used to inject the medium or hydrogel into the microfluidic channel underneath the porous membrane. The microporous SU-8 membrane (Part 3) formed the barrier between the middle well in Part 2 and the volume below it in the microfluidic channel (Part 4). The SU-8 membrane was sandwiched between the PDMS structures when the device was assembled. Part 5 in the bottom of the device was a glass cover slip (170 μm thick square with a side of 22 mm, Zeiss), which enabled confocal imaging. When the cell culture device was used for preparing samples for scanning electron microscope (SEM) imaging, thicker glass plates (1 mm thick square with a side of 49 mm) were used instead of the coverslips. The glass parts also made the device more rigid. All parts were bonded together using oxygen plasma for 20 s at 30 W in 0.3 mbar pressure (Pico, Diener electronic GmbH and Co., KG, Ebhausen, Germany).

2.2. Membrane fabrication and assembly on the device

The SU-8 membranes were fabricated as a patch of 20 samples on top of a four-inch silicon wafer. SU-8 material was patterned using UV lithography. This method allows exact placement of the pores in the membrane. Four types of pores were tested: a 10 μm $\times$ 5 μm slit, an 8 μm x 8 μm square, a 10 μm diameter circle and an 8 μm diameter circle (P1-P4 in figure 1(d)). The pores were placed in a grid formation with a 100 μm separation distance in four sectors (S1-S4 in figure 1(c)) in the middle of the membrane. This separation distance was chosen in order to leave room for wiring which is needed to connect to the electrodes that we have planned to

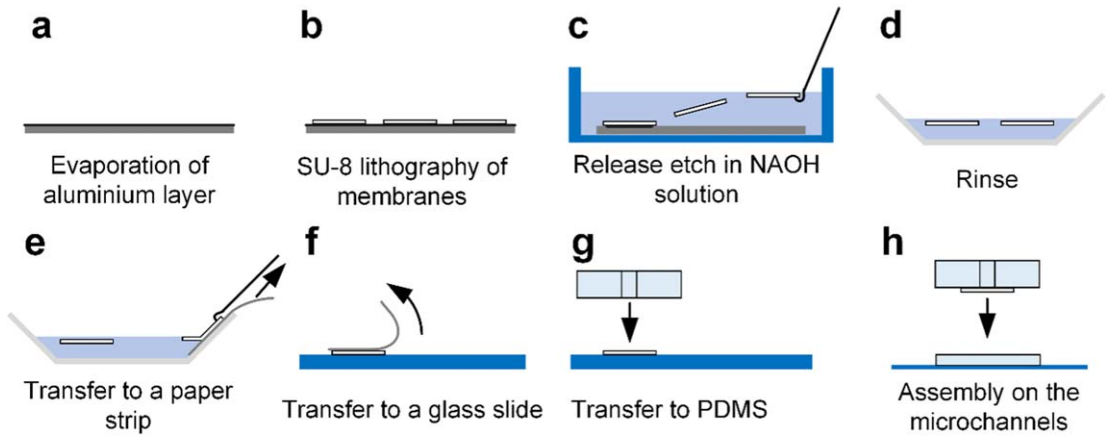

Figure 2. The fabrication of the membranes and their assembly on the PDMS cell culture device.

incorporate to this design in the future. The rest of the membrane was filled with a grid of circular pores (∅10 μm, 100 μm separation) to make the release etching more consistent. In addition, a circular hole (∅1.6 mm) was included in the edge of the membrane to ease up the pickup from the etch solution using a metallic hook tool when the membrane was released from the substrate. The design also has annotation markings to identify each membrane and to help to distinguish the orientation of the membrane during the assembly process (figure 1(b)). In addition, a quality control test pattern was added in the middle of the membrane. It contained both circular (T1-T2) and rectangular pores (T3-T4) whose dimensions were increased by a 1 μm interval (figure 1(c)).

The membranes were made of SU-8 5 material (Microchem, USA) on a silicon wafer (University Wafer, Boston, MA, USA) using UV photolithography. First, the wafer was coated with an e-beam evaporated 30 nm thick sacrificial aluminium layer (figure 2(a)) using an Orion BC-3000 series box coater (System Control Technologies) equipped with a Telemark 246 e-beam source. Next, the wafer was treated with oxygen plasma (30 W, 2 min) (Vision 320 Mk II RIE, Advanced Vacuum, Malmö, Sweden) to improve the adhesion of the SU-8 layer that was spin-coated over the aluminium layer (4000 rpm, 40 s). This procedure was based on the parameters used in [32] and resulted in 3.5 μm thick membranes. The wafer was subsequently soft baked on a hot plate (1 min at 65 °C and 3 min at 95 °C) and was allowed to cool to room temperature. The wafer and SU-8 layer were exposed (7.15–7.25 mW cm^{-2} UV source, 12 s) through a chrome mask. The parameter values used were determined experimentally. After the post-exposure bake on a hot plate (1 min at 65 °C and 2 min at 95 °C), the SU-8 membranes were developed for 4 min with an MR-DEV 600 developer (Microchem) using ultrasonic agitation. Finally, the SU-8 membranes on the wafer were post baked in an oven (150 °C, 15 min). After these fabrication steps, the patterning of the membranes was finished (figure 2(b)).

The membrane was released by etching the aluminium layer with NaOH solution (1 mol). The membranes were lifted from the solution using a metallic hook tool (figure 2(c)). Next, the membranes were rinsed with NaOH solution (0.1 mol) and deionized water (figure 2(d)). The wet membranes were transferred to a microscope glass slide utilizing pervious fibre strips (figures 2(e)–(f)). The membranes typically stretched out on the water surface, and the pervious fibre strips allowed easy handling and reduced the wrinkling of the membranes. Next, the PDMS wells part was gently placed on the membrane (figure 2(g)) to pick it up from the glass. Finally, the PDMS wells and the membrane were assembled with the other parts of the device (figure 2(h)).

2.3. Cell culture methods

The fabricated porous membranes were tested by using human neurons. The neurons were differentiated from the in-house-derived hiPSC line 10212.EURCCs (total passages 31, feeder free passages 6) [37]. The Faculty of Medicine and Health Technology (MET), Tampere University, Finland, has approval supportive statements from the regional ethics committee of the Pirkanmaa Hospital District for the derivation, culture, and differentiation of hiPSCs (R08070). The HiPSCs were cultured according to a previously published protocol [38]. According to the protocol, the hiPSCs were transferred to feeder-free culture using recombinant human laminin-521 (LN521, Biolamina, Sweden) and E8 medium (Thermo Fisher Scientific). Thereafter, the hiPSCs were differentiated into cortical neurons according to a previously published protocol that produces highly pure neuronal populations that show the formation of functional neuronal networks [34]. Briefly, the differentiation consisted of three phases: neural induction (Days 0–12), neural proliferation (Days 13–25) and neural

maturation (Day 26 onwards). On Day 32 of differentiation, the cells were detached and plated onto SU8 membranes.

Before the cell experiments, the devices were disinfected by dipping them in 70% ethanol and washing them with Dulbecco's phosphate buffered saline (PBS). The top side of the SU-8 membranes was coated with LN521 (30 μg ml^{-1}) for two hours in a cell culture incubator at 37 °C in a humified environment. Neuronal cells were plated at a density of 70900 cells cm^{-2} on the devices on top of the membranes. Cell handling was performed according to a published protocol [34]. Neural maintenance medium (NMM) was used as a basal medium, which consisted of 1:1 DMEM/F12 with Glutamax and Neurobasal, 0.5% N2, 1% B27 with retinoic acid, 0.5 mM GlutaMAX, 0.5% non-essential amino acid (NEAA), 50 μM 2-mercaptoethanol (all from Thermo Fisher Scientific), 2.5 μg ml^{-1} insulin (Sigma) and 0.1% penicillin/streptomycin (Thermo Fisher Scientific). NMM was supplemented using 20 ng ml^{-1} brain-derived neurotrophic factor (BDNF, R&D Systems), 10 ng/ml glial-derived neurotrophic factor (GDNF, R&D Systems), 500 μM dibutyryl-cyclicAMP (db-cAMP, Sigma) and 200 μM ascorbic acid (AA, Sigma). In the plating step, in single cell suspension and during the first day of culturing on membranes, the NMM medium was supplemented with 2 μl ml^{-1} ROCK inhibitor (Y-27632, Sigma) to minimize the cell death caused by the detaching process. During culturing, the medium was changed every two to three days. Cell cultures were analysed 1, 3 and 7 days after plating cells on the membrane, and the timepoints are referred to as days *in vitro* (DIV), DIV1, DIV3 and DIV7, respectively.

2.4. SEM imaging

The images of the membranes and the cells were acquired either by field emission SEM (FESEM; ULTRAplus Carl Zeiss, Oberkochen, Germany) or tungsten-filament SEM (Tescan Vega, Bruker). First, the quality of the pores was characterized using a membrane sample without cells. Subsequently, six neuronal cultures in the designed devices were prepared for SEM imaging, with two parallel samples for each time point (DIV1, DIV3 and DIV7). The samples were fixed using 5% glutaraldehyde for 60 min, followed by dehydration using an increasing ethanol series (10%, 20%, 40%, 60%, 80%, 99.5%, v/v of EtOH) for 10 min each and air-drying overnight. The SU-8 membranes with cells were detached from the devices for SEM imaging. To avoid charging, the samples were attached to SEM aluminium stubs with carbon tape in the following manner. A piece of double-sided conductive adhesive was attached to the side of the membrane where the cells were plated. Then, a circular part under the tape was cut from the sample and fixed to a metallic holder. In this way, the bottom side where neurites migrated through the membrane was ready for SEM imaging. This sample preparation is a delicate process, and some membranes were torn. Before SEM scanning, the membrane sample without cells was sputter-coated with a carbon layer, while the cell samples were sputter-coated with a gold layer.

For the analysis, the low magnification SEM images were divided into 0.12 mm^2 sample areas (4 by 5 pore grid/sample) for further analysis. The quality of the images was adequate for calculating (1) the number of pores via which the neurites transferred through the membrane and (2) the number of neurons on the bottom side of the membrane. The pores containing interpenetrating neurites were named neurite-occupied pores, and their percentage was calculated (each analysed sample area contained 20 pores, 4–8 sample areas per design was analysed). In addition, the number of traversed neurons was calculated from the same sample areas. The number of analysed sample areas per sector type is given in the supplementary table 1. Statistical analysis was performed using GraphPad Prism 5, version 5.02 (GraphPad Software Inc., California, USA). Analysis was performed using a non-parametric Kruskal-Wallis statistical test followed by Dunn's post hoc test. A p value > 0.05 was considered significant.

2.5. Immunocytochemistry and confocal imaging

To verify the neuronal phenotype, the cultures were stained against neuronal markers using an immunocytochemical protocol published earlier [39]. Cells were fixed with 4% paraformaldehyde for 30 min and washed twice with PBS and blocked with 10% normal donkey serum, 0.1% Triton X-100, and 1% bovine serum albumin in phosphate saline puffer (PBS) for 60 min. After blocking, the samples were washed once with 1% normal donkey serum (Sigma), 0.1% Triton X-100, and 1% bovine serum albumin (BSA) in PBS, which was also used in primary antibody incubation. Primary antibodies against β-tubulin III (mouse IgG, 1:1000, Sigma) and MAP2 (rabbit, 1:600, Millipore, Burlington, MA, USA) were incubated with samples overnight at +4 °C on a shaker. Samples were washed with 1% BSA in PBS two times. Secondary antibodies Alexa Fluor 488 (anti-rabbit IgG, 1:400 Life Technologies) and Alexa Fluor 568 (anti-mouse IgG, 1:400, Life Technologies) were diluted in 1% BSA in PBS and incubated with samples for two hours. Thereafter, samples were washed four times with PBS and mounted with Vectashield mounting medium containing 4′,6-diamidino-2-phenylindole (DAPI, Vector Laboratories, Burlingame, CA, USA). Samples were imaged with a Zeiss Cell Observer.Z1 inverted microscope equipped with a Zeiss LSM 780 confocal unit (Carl Zeiss AG) using a Zeiss Plan Apo 10x/0.45, WD 2 mm (Air) objective lens. The images were deconvolved with Huygens Essentials deconvolution

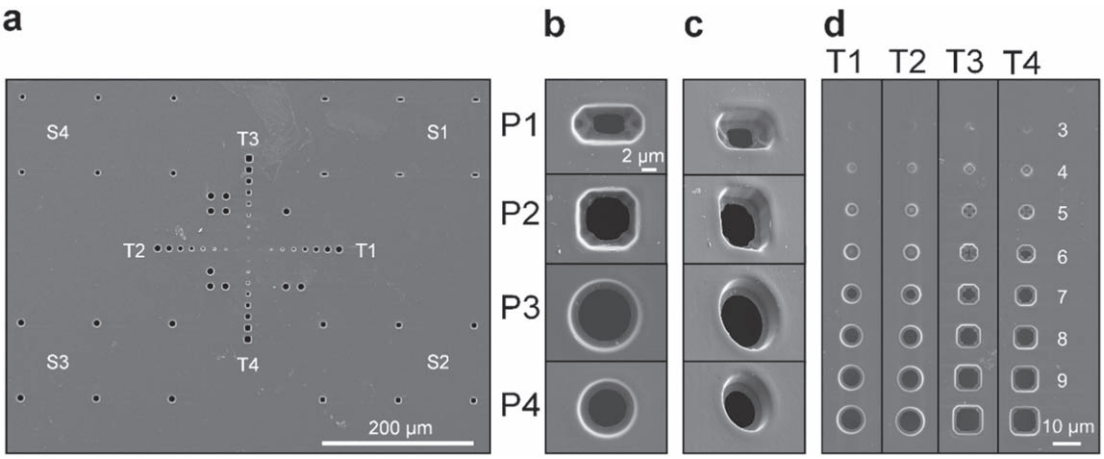

Figure 3. (a) A SEM image of a quality control test pattern in the middle of a fabricated membrane and the corners of the opening grids. (b) SEM images of the openings from the top. (c) The openings seen from an angle. (d) Magnified images of the test sites (T1-T4) of the quality control pattern. The pores pass through the membrane when the size of the pore design is at least 7 μm.

software (Scientific Volume Imaging, Hilversum, Netherlands), and the colour channels were combined using ImageJ (NIH, Bethesda, MA, USA). Representative low magnification images were taken from all sections, and two parallel samples were imaged from each timepoint (DIV1, 3 and 7).

3. Results and discussion

3.1. Microfabricated porous membranes

The quality of the fabricated SU-8 membrane patch was evaluated by examining a sample membrane with SEM before the cell culture experiments (figure 3(a)). All the pore shapes P1 to P4 were uniform within each sector in the tested sample. SEM images of the tested pore types (P1-P4) taken normal to the top are shown in figure 3(b), and those taken at a tilted angle are shown in in figure 3(c). Pores P2 to P4 formed nearly as designed. However, the fabrication process resulted in a lip that reduced the actual dimensions of the pore. The smallest inner dimensions of the pores in figure 3(b) are 2.9 μm by 4.4 μm (P1), 6.1 μm (P2), 7.4 μm (P3) and 5.4 μm (P4). The effect that caused the lip disfigured the shape of Pore P1. However, the residual opening of this pore was the smallest gained in this study. One possible cause of this lip might be the metallic sacrificial layer which has good thermal conductivity.

The minimum possible pore size was evaluated by examining the quality control test pattern (T1-T4, figure 3(d)). Here, the pores passed through the membrane only when the diameter of the designed circular pore was 7 μm or larger (T1 and T2). Circular pores with a diameter of 6 μm or smaller only formed a depression in the membrane. This situation was similar to that of the square-shaped pores (T3 and T4). However, the square in T4 appeared to be partially open even when its side length was only 6 μm.

Quirós-Solano *et al* stated that patterning reliably features smaller than 5 μm in polymeric materials may still be cumbersome [7]. This reliability problem is emphasized when multiple membranes are processed simultaneously on large diameter wafers. The fabrication parameters can be adjusted with the methods suggested by Keller *et al* [40]. However, the thickness of the membrane will always limit the minimum pore size, and in practice, very precise process parameters are difficult to reproduce. By making membranes thinner, we could fabricate even smaller pores, as demonstrated by Kim *et al* [26]. However, the edges of the smallest pores tested by the authors of that study (actual diameter was approximately 1 μm) were severely deformed. The method tested in our work did not result in as small pore sizes as Warkiani *et al* achieved with the method which utilized different polymers as a sacrificial layer [28]. The thickness and the processing parameters of SU-8 were similar in these two studies. We fabricated self-supporting patterned SU-8 membranes on top of a metallic sacrificial layer in a similar way as shown in the methods used by Viveros *et al* to fabricate flexible electronics [20] or by Feiner *et al* to fabricate cardiac patches with multifunctional electronics [19]. Here, we chose to use aluminium as a sacrificial layer instead of nickel to avoid using acids and cleaning the residues after release etching. Moreover, our approach enabled to avoid the use of polymer or soap-based release layers [26] which limit processing options such as patterning conductors on the membrane with photolithography as this is our aim in the future.

The fabrication method proposed here only required regular single-layer UV lithography. Kim *et al* and as Warkiani *et al* used additional supporting structures on their membranes. These additional layers have some

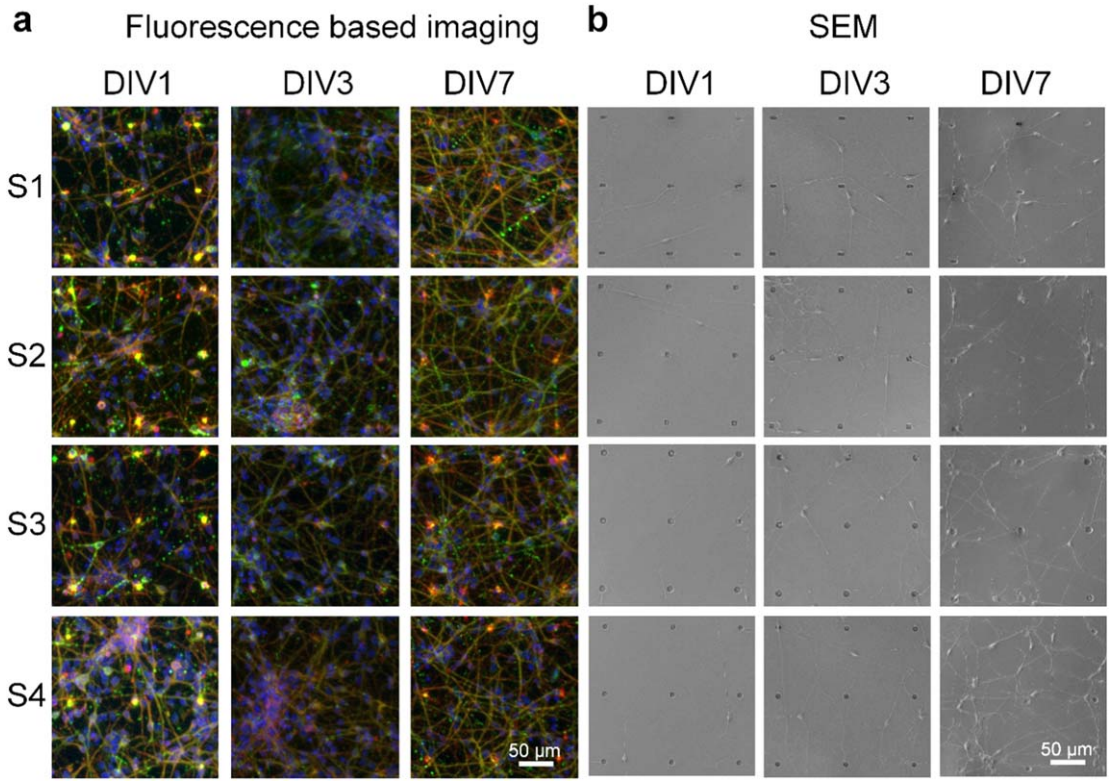

Figure 4. The overall cell and the neurite growth on the SU-8 membranes. (a) Fluorescence based images of the culture on the top side of the SU-8 membrane. (b) SEM images of each sector on the bottom of the membrane. Blue: DAPI, green: MAP-2 and red: β-tubulin$_{III}$

disadvantages due to increased relief. For example, they may hinder large area imaging and the connectivity of the neuronal networks on the surfaces of the membrane.

3.2. Feasibility of membranes for hiPSC-derived neuronal models

The target cell type and end-user application must be taken into account when determining the suitable pore size or selecting the fabrication methods and materials. The largest diameter of pores (10 μm) was selected as the upper limit in this study because preliminary experiments showed an extensive traverse of single cells through 15 μm pores to the bottom part of the cell culture device during cell plating (data not shown). In contrast, membranes with pore diameters of 10 μm and smaller were able to keep the cells on the top side during cell plating and would thus suite for innervating the tissue under the membrane. These membranes can be utilized as supportive or selective barriers in multi-tissue blocks in addition to innervation. The minimum pore size was set by the limitations of the available fabrication method.

Functionality and cell compatibility analyses were performed at time points DIV1, 3 and 7. Overall, the SU-8 material used in this study showed good cytocompatibility with human neurons. The neuronal phenotype and neuronal network morphology were studied using immunocytochemical staining against neuronal markers MAP-2 and β-tubulin III. Cells growing on top of the SU-8 membrane expressed neuronal markers at all studied time points, indicating that the SU-8 material did not have negative effects on neuronal maturation (figure 4(a)). This issue had to be confirmed before further development since the literature presents some concerns about the cytotoxicity of SU-8 materials [41, 42]. The fabrication parameters, such as baking temperature and time or the thickness of the membrane can potentially cause cytotoxicity. At DIV1, the neurons showed good attachment to the membrane and started to spread on the surface, while neurites grew randomly oriented along the membrane. During culturing, the neuronal network became more complex and interconnected over time (figure 4(a)). At DIV7, the neurons formed a strong interconnected network on top of the membrane. Slight clustering of neuronal cells was observed at DIV7, which is a typical phenomenon in neuronal cultures in general [43]. The embedded pores did not affect neuronal network formation on top of the membrane and all sectors showed equal network development (figure 4(a)).

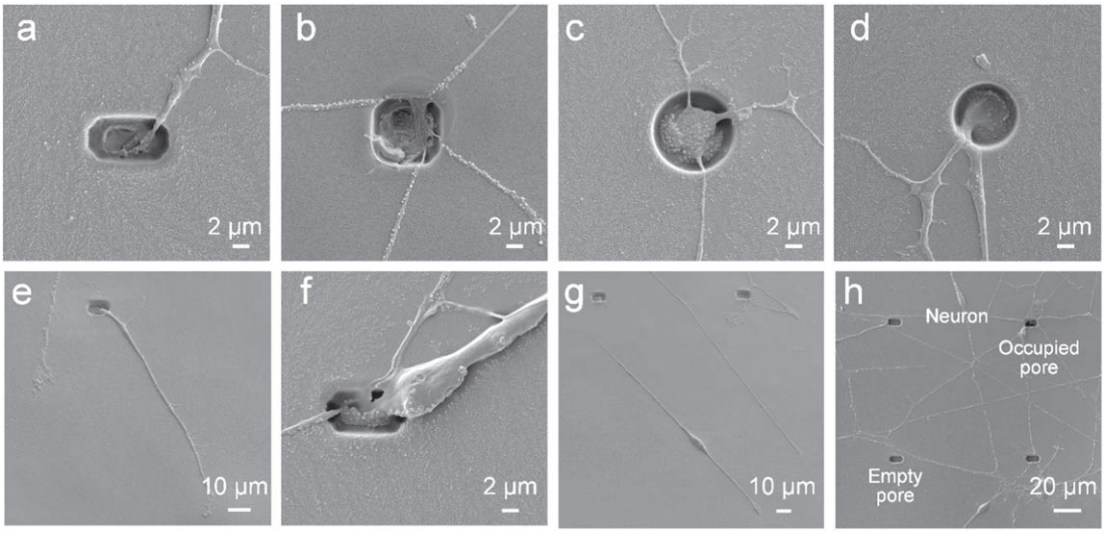

Figure 5. Detailed SEM images of neurites on the bottom side of the membrane. (a)–(d) Examples of the neurites in each tested pore types (P1-P4) at DIV1. (e) A neurite protruding through the membrane from the seeding side to the opposite side of the membrane (DIV1).(f) An example of a neuron migrating through the opening at DIV1. (g) Unconnected neuron on the bottom side of the membrane (DIV1). (h) Neurite network on bottom of the mebrane at DIV7.

3.3. Analysis of neurites and neurons on the bottom side of the membrane with SEM

Neurons were plated on the top side of the membrane, and neurite or neuron migration through the pores to the bottom side was studied on DIV1, 3 and 7. The aim was test the effects of the different size pores on the neuron and theirs processes migration through the pores. In the ideal case, the pores restrict the migration of neuronal cells from the top side while allowing neurites to grow through the pores. Figure 4(b) gives an overview of the cell growth on the bottom side of the membrane. The pores did not restrict the neurites and they were observed in each sector at DIV 1. Figures 5(a)–(d) presents higher magnification images of neurites crossing the pores at DIV1. Moreover, figure 5(e) illustrates a single neurite growing from the top to the bottom side through a pore. Most of the observed neurites had a straight elongated shape and were connected to the pores, but they did not have many connections to the other neurites at DIV1.

Unfortunately, the pores could not fully restrict the migration of the neurons. However, compared to the massive number of neurons on top of the membrane in phase contrast images (supplementary figure 2), only a few neurons were observed at DIV1 on the bottom side of the membrane in SEM images (figure 4(b)). Migration of a single neuron through a pore is represented in figure 5(f). In addition, some totally disconnected neurons were observed (figure 5(g)). At DIV3, SEM images show that the neurites possessed more complex morphologies and started to form sparse networks on the bottom side of the membrane (figure 4(b)). Even more complex and dense networks were formed by DIV7 (figures 4(b) and 5(h)).

A more comprehensive numerical assessment of the neurites and neurons on the bottom side of the membrane and the effect of the different pores was performed using SEM images from each sector. The percentage of occupied pores and the number of observed neurons per area are given in figure 6. Example cases are shown in figure 5(h).

The number of occupied pores was the lowest at DIV 1. The median percentage values for Sectors S1 to S4 were 45.0, 55.0, 40.0 and 20.0, respectively. The majority of pores were already occupied by DIV3 (median percentages: 70.0, 87.5, 92.5, and 75.0 for S1 to S4, respectively), with significantly more pores occupied in S3 than in S1 (p value: 0.0429). There was a slight decrease in the percentage of neurite-occupied pores on DIV7 (medians 45.0, 70.0, 82.5, and 80.0 for S1 to S4, respectively), but the formed neurite networks were more pronounced than those on DIV3 (figure 4(b)).

At DIV1, the number of neurons that migrated to the bottom side was low (figure 6(b)) and very similar between all sectors (medians per 0.12 mm^2: 4.5, 7.0, 4.0, and 2.0 for S1 to S4, respectively). Between DIV1 and DIV3, the number of neurons (figure 6(b)) increased on the bottom side of the membrane. At the later timepoints of DIV3 (medians per 0.12 mm^2: 12.0, 25.0, 23.5, and 12.5 for S1 to S4, respectively) and DIV7 (medians 11.0, 19.0, 30.5, and 27.0 for S1 to S4, respectively), S1 had the lowest number of neurons, and S3 had the highest number of neurons, with the difference being statistically significant at DIV7 between S1 and S3 (p value: 0.0026). Even though S3 had the highest number of neurons on the bottom side, meaning it had the weakest design as a restrictor, it was the design that facilitated the most abundant neurite growth through the pores. It can be concluded that the number of neurons that migrated to the bottom side of the membrane

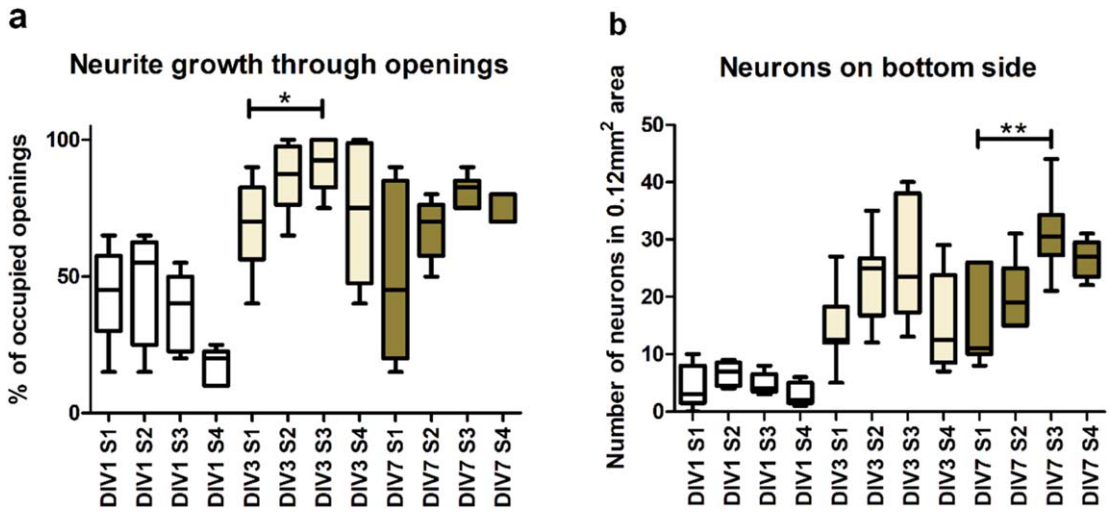

Figure 6. Numerical analysis of the number of neurite ocupied pores and number of neurons that migrated through openings to the bottom side of the membrane. (a) Boxplot showing the percentage of occupied openings that had visible neurite growth in different designs (S1–4) at the analysed timepoints (DIV1, 3 and 7). (b) Boxplot showing the number of neurons in the bottom side of the membrane. DIV: days *in vitro*. Number of analysed areas (0.12 mm^2) per section type is between 5–8 per group counted from two parallel samples. $^{*} = p < 0.05$ and $^{**} = p < 0.01$

(figure 6(b)) and the density of the neuronal network on the bottom side (figure 4(b)) followed similar trends: both increased over time, whereas the percentage of neurite-occupied pores slightly decreased at DIV7.

We were able to achieve partial neuronal axonal isolation with the investigated pore sizes and shapes. Their number in the bottom side was substantially smaller than the number of cells plated on top of the membrane (85 neurons per 0.12 mm^2 area, 709 cells/mm^2), especially in the case of Pore 1 (at DIV7 median of 11 per 0.12 mm^2, 92 cells/mm^2).

In comparison to our study, neuronal soma separation has been studied before in an article by George *et al* using neuroplastoma cells, e.g., SY-SY5Y, and highly porous track-etched membranes with random pore localization [5]. The thickness of the membranes of George *et al* was between 20 and 25 μm, which is almost six times thicker than the membranes prepared in our study. The thickness of the restricting structures affects the migration and must be taken into account. In addition, it should be noted that the density of the pores in the membranes prepared by George *et al* was much higher in comparison with that in our work. The cell type and cell plating density influence axonal penetration and soma restriction as well. George *et al* reported cell penetration of 72 $\pm$ 20 cells/mm^2 for 3 μm diameter pores. In addition, their study showed that 1.2 μm pores were axonal permissive and soma restrictive with SY-SY5Y cells. Thus, our results are in line with the previous results. Both of these methods are similar to the transwell assays that are a common tool for studying cell migration. Overall, we see that our current work can offer additional information on the migration of hiPSC-derived neurons since human neuronal cells are under-represented in the traswell studies and the usage of other than thick track-etched membranes are rarity.

In summary, we showed that neurons can be successfully cultured on top of the SU-8 membranes for at least seven days. Neurites were able to find the pores and penetrate through to the underlying compartment. This suggests that the membranes may be used in the innervation applications. In our model, the pore size had an effect on the neuronal network forming on the bottom side of the membrane, and thus, the selection of the pore size can be used to modify the model such that it supports study-specific research questions. The pore size influences both neurite and neuronal cell growth through the pores. Increasing the pore diameter increases the neurite growth through the pores but also allows the migration of neurons to the bottom side, resulting in low selectivity. Strong neuronal networks on both sides of the membrane with lower soma separation properties can be used, e.g., to study electrical activity or innervation in cases where a small degree of cell migration has negligible effects on the results. A smaller pore size produces a sparser neurite network but offers better soma separation properties. The smaller pore size is beneficial in such research questions where neuronal somas interfere with the analysis. The full axonal isolation requires smaller pores. It is unclear if normal UV lithography is suited for reliably making small enough pores. Alternatively, the other isolation methods such as tunnels can be used in combination with membranes to achieve better axonal isolation.

4. Conclusions

We fabricated cell culture devices with porous self-supporting single-layer SU-8 membranes for hiPSC neurons. The fabrication method allowed us to customize of the pore size and location. The method proposed in this paper provides additional benefits. The tested aluminum release layer can be easily removed and it does not leave messy residues. The release layer is also compatible with many microfabrication processes and thus allows the future development of the membrane by adding sensors such as MEAs in the membrane. We also developed a method for handling the thin membranes without using supporting structures on the membranes. Thick additional layers or walls may disturb optical imaging and the cell connectivity on the surfaces. Importantly, this study was conducted with human neurons derived from human pluripotent stem cells. As the most of the studies conducted earlier have utilized rodent and cancer derived neurons, they do not directly translate in the high need of developing human cell-based models. There are crucial cellular and behavioral differences in neurons depending of their origin, which states for the need to test novel technologies with the desired cell type, that is, human neurons. The thin porous SU-8 material was found to provide very good cytocompatibility with hiPSC neurons and we were able to achieve partial, but still significant, axonal isolation. The results suggest that innervation of tissue blocks placed underneath the membrane is achievable due to neurite growth through the pores. Next step will be to increase the functionality of the interface by integrating sensing elements into the membrane.

Acknowledgments

The authors acknowledge the Biocenter Finland (BF)-funded Tampere Imaging Facility (TIF) and Tampere Microscopy Center for their services.

Data availability statement

The data that support the findings of this study are available upon reasonable request from the authors.

Funding

The reported study was funded by Academy of Finland Centre of Excellence in Body-on-Chip Research.

Ethical statement

There are no conflicts to declare.

ORCID iDs

T Salpavaara https://orcid.org/0000-0002-6331-6972

References

[1] Millet L J, Stewart M E, Nuzzo R G and Gillette M U 2010 Guiding neuron development with planar surface gradients of substrate cues deposited using microfluidic devices *Lab Chip* **10** 1525
[2] Jokinen V, Sakha P, Suvanto P, Rivera C, Franssila S, Lauri S E and Huttunen H J 2013 A microfluidic chip for axonal isolation and electrophysiological measurements *J. Neurosci. Methods* **212** 276–82
[3] Pasman T, Grijpma D, Stamatialis D and Poot A 2018 Flat and microstructured polymeric membranes in organs-on-chips *J. R. Soc. Interface* **15** 20180351
[4] Taylor A M, Blurton-Jones M, Rhee S W, Cribbs D H, Cotman C W and Jeon N L 2005 A microfluidic culture platform for CNS axonal injury, regeneration and transport *Nat. Methods* **2** 599–605
[5] George J H, Nagel D, Waller S, Hill E, Parri H R, Coleman M D, Cui Z and Ye H 2018 A closer look at neuron interaction with track-etched microporous membranes *Sci. Rep.* **8** 15552
[6] Chung H H, Mireles M, Kwarta B J and Gaborski T R 2018 Use of porous membranes in tissue barrier and co-culture models *Lab Chip* **18** 1671–89
[7] Quirós-Solano W F *et al* 2018 Microfabricated tuneable and transferable porous PDMS membranes for Organs-on-Chips *Sci. Rep.* **8** 13524
[8] Maoz B M *et al* 2018 A linked organ-on-chip model of the human neurovascular unit reveals the metabolic coupling of endothelial and neuronal cells *Nat. Biotechnol.* **36** 865–74
[9] Huh D (D) 2015 A human breathing lung-on-a-chip *Ann. Am. Thorac. Soc.* **12** S42–4
[10] Booth R and Kim H 2012 Characterization of a microfluidic *in vitro* model of the blood-brain barrier (μBBB) *Lab Chip* **12** 1784–92

[11] Kim H J, Huh D, Hamilton G and Ingber D E 2012 Human gut-on-a-chip inhabited by microbial flora that experiences intestinal peristalsis-like motions and flow *Lab Chip* **12** 2165
[12] Virlogeux A, Moutaux E, Christaller W, Genoux A, Bruyère J, Fino E, Charlot B, Cazorla M and Saudou F 2018 Reconstituting corticostriatal network on-a-chip reveals the contribution of the presynaptic compartment to huntington's disease *Cell Rep.* **22** 110–22
[13] Toivanen M, Pelkonen A, Mäkinen M, Ylä-Outinen L, Sukki L, Kallio P, Ristola M and Narkilahti S 2017 Optimised PDMS tunnel devices on MEAs increase the probability of detecting electrical activity from human stem cell-derived neuronal networks *Front. Neurosci.* **11** 00606
[14] Silva D I, Santos B P, dos, Leng J, Oliveira H and Amédée J 2017 Dorsal root ganglion neurons regulate the transcriptional and translational programs of osteoblast differentiation in a microfluidic platform *Cell Death Dis.* **8** 3209
[15] Sakai K, Shimba K, Ishizuka K, Yang Z, Oiwa K, Takeuchi A, Kotani K and Jimbo Y 2017 Functional innervation of human induced pluripotent stem cell-derived cardiomyocytes by co-culture with sympathetic neurons developed using a microtunnel technique *Biochem. Biophys. Res. Commun.* **494** 138–43
[16] Park D, Lee J, Chung J J, Jung Y and Kim S H 2020 Integrating organs-on-chips: multiplexing, scaling, vascularization, and innervation *Trends Biotechnol.* **38** 99–112
[17] Heiduschka P, Romann I, Stieglitz T and Thanos S 2001 Perforated microelectrode arrays implanted in the regenerating adult central nervous system *Exp. Neurol.* **171** 1–10
[18] Musick K, Khatami D and Wheeler B C 2009 Three-dimensional micro-electrode array for recording dissociated neuronal cultures *Lab Chip* **9** 2036–42
[19] Feiner R, Engel L, Fleischer S, Malki M, Gal I, Shapira A, Shacham-Diamand Y and Dvir T 2016 Engineered hybrid cardiac patches with multifunctional electronics for online monitoring and regulation of tissue function *Nat. Mater.* **15** 679–85
[20] Viveros R D, Zhou T, Hong G, Fu T-M, Lin H-Y G and Lieber C M 2019 Advanced one- and two-dimensional mesh designs for injectable electronics *Nano Lett.* **19** 4180–7
[21] Rios G, Lubenov E V, Chi D, Roukes M L and Siapas A G 2016 Nanofabricated neural probes for dense 3D recordings of brain activity *Nano Lett.* **16** 6857–62
[22] Demircan Yalcin Y and Luttge R 2021 Electrical monitoring approaches in 3-dimensional cell culture systems: toward label-free, high spatiotemporal resolution, and high-content data collection *in vitro Organs-on-a-Chip* **3** 100006
[23] Apel P 2001 Track etching technique in membrane technology *Radiat. Meas.* **34** 559–66
[24] Budhwani K I, Thomas V and Sethu P 2016 Lab-on-a-brane: nanofibrous polymer membranes to recreate organ–capillary interfaces *J. Micromechanics Microengineering* **26** 035013
[25] Esch M B, Sung J H, Yang J, Yu C, Yu J, March J C and Shuler M L 2012 On chip porous polymer membranes for integration of gastrointestinal tract epithelium with microfluidic 'body-on-a-chip' devices *Biomed. Microdevices* **14** 895–906
[26] Kim M Y, Li D J, Pham L K, Wong B G and Hui E E 2014 Microfabrication of high-resolution porous membranes for cell culture *J. Memb. Sci.* **452** 460–9
[27] Zheng S, Lin H, Liu J-Q, Balic M, Datar R, Cote R J and Tai Y-C 2007 Membrane microfilter device for selective capture, electrolysis and genomic analysis of human circulating tumor cells *J. Chromatogr.* A **1162** 154–61
[28] Warkiani M E, Lou C P and Gong H Q 2011 Fabrication and characterization of a microporous polymeric micro-filter for isolation of Cryptosporidium parvum oocysts *J. Micromechanics Microengineering* **21** 035002
[29] Kuiper S, Van Rijn C J M, Nijdam W and Elwenspoek M C 1998 Development and applications of very high flux microfiltration membranes *J. Memb. Sci.* **150** 1–8
[30] Ma S H, Lepak L A, Hussain R J, Shain W and Shuler M L 2005 An endothelial and astrocyte co-culture model of the blood-brain barrier utilizing an ultra-thin, nanofabricated silicon nitride membrane *Lab Chip* **5** 74–85
[31] Cheng Y, Zhu S and Pang S W 2021 Directing osteoblastic cell migration on arrays of nanopillars and nanoholes with different aspect ratios *Lab Chip* **21** 2206–16
[32] Ristola M, Sukki L, Azevedo M M, Seixas A I, Relvas J B, Narkilahti S and Kallio P 2019 A compartmentalized neuron-oligodendrocyte co-culture device for myelin research: design, fabrication and functionality testing *J. Micromechanics Microengineering* **29** 65009
[33] Ristola M, Fedele C, Hagman S, Sukki L, Kapucu F E, Mzezewa R, Hyvärinen T, Kallio P, Priimagi A and Narkilahti S 2021 Directional growth of human neuronal axons in a microfluidic device with nanotopography on azobenzene-based material *Adv. Mater. Interfaces* **8** 2100048
[34] Hyvärinen T, Hyysalo A, Kapucu F E, Aarnos L, Vinogradov A, Eglen S J, Ylä-Outinen L and Narkilahti S 2019 Functional characterization of human pluripotent stem cell-derived cortical networks differentiated on laminin-521 substrate: comparison to rat cortical cultures *Sci. Rep.* **9** 17125
[35] Heikkilä T J, Ylä-Outinen L, Tanskanen J M A, Lappalainen R S, Skottman H, Suuronen R, Mikkonen J E, Hyttinen J A K and Narkilahti S 2009 Human embryonic stem cell-derived neuronal cells form spontaneously active neuronal networks *in vitro Exp. Neurol.* **218** 109–16
[36] Meijer M *et al* 2019 A single-cell model for synaptic transmission and plasticity in human iPSC-derived neurons *Cell Rep.* **27** 2199–2211.e6
[37] Kiamehr M, Klettner A, Richert E, Koskela A, Koistinen A, Skottman H, Kaarniranta K, Aalto-Setälä K and Juuti-Uusitalo K 2019 Compromised barrier function in human induced pluripotent stem-cell-derived retinal pigment epithelial cells from type 2 diabetic patients *Int. J. Mol. Sci.* **20** 3773
[38] Hongisto H, Ilmarinen T, Vattulainen M, Mikhailova A and Skottman H 2017 Xeno- and feeder-free differentiation of human pluripotent stem cells to two distinct ocular epithelial cell types using simple modifications of one method *Stem Cell Res. Ther.* **8** 291
[39] Ylä-Outinen L, Harju V, Joki T, Koivisto J T, Karvinen J, Kellomäki M and Narkilahti S 2019 Screening of hydrogels for human pluripotent stem cell–derived neural cells: hyaluronan-polyvinyl alcohol-collagen-based interpenetrating polymer network provides an improved hydrogel scaffold *Macromol. Biosci.* **19** 1–13
[40] Keller S, Blagoi G, Lillemose M, Haefliger D and Boisen A 2008 Processing of thin SU-8 films *J. Micromechanics Microengineering* **18** 125020
[41] Vernekar V N, Cullen D K, Fogleman N, Choi Y, García A J, Allen M G, Brewer G J and LaPlaca M C 2008 SU-8 2000 rendered cytocompatible for neuronal bioMEMS applications *J. Biomed. Mater. Res. Part* A **89** 138–51
[42] Nemani K V, Moodie K L, Brennick J B, Su A and Gimi B 2013 *In vitro* and *in vivo* evaluation of SU-8 biocompatibility *Mater. Sci. Eng.* C **33** 4453–9
[43] Sun Y, Huang Z, Liu W, Yang K, Sun K, Xing S, Wang D, Zhang W and Jiang X 2012 Surface coating as a key parameter in engineering neuronal network structures *in vitro Biointerphases* **7** 29